XV International Conference on Computational Plasticity. Fundamentals and Applications
COMPLAS 2019
E. Oñate, D.R.J. Owen, D. Peric, M. Chiumenti & Eduardo de Souza Neto (Eds)

CRYSTAL PLASTICITY FINITE ELEMENT SIMULATIONS OF CAST α-URANIUM

NICOLÒ GRILLI*, ALAN C.F. COCKS* AND EDMUND TARLETON†

* Department of Engineering Science
University of Oxford
Parks Road, OX1 3PJ, UK
e-mail: nicolo.grilli@eng.ox.ac.uk, web page: http://www2.eng.ox.ac.uk/solidmech/

† Department of Materials
University of Oxford
Parks Road, OX1 3PH, UK
e-mail: edmund.tarleton@materials.ox.ac.uk - Web page: https://omg.web.ox.ac.uk

Key words: Uranium, Crystal Plasticity, Finite Element method, Twinning, Thermal residual strains

Abstract. α-uranium, the stable phase of uranium up to 670°C, has a base-centred orthorombic crystal structure. This crystal structure gives rise to elastic and thermal anisotropy, meaning α-uranium exhibits complex deformation and fracture behaviour. Understanding the relationship between the microstructure and mechanical properties is important to prevent fracture during manufacture and usage of components. The lattice of α-uranium corresponds to a distorted close-packed-hexagonal crystal structure and it exhibits twins of both the 1st and 2nd kind. Therefore, detailed examination of the behaviour of α-uranium can also contribute to the general understanding of the interaction between plasticity, twinning and fracture in hcp crystals. Plastic deformation in α-uranium can be accommodated by 4 slip systems and 3 twin systems, previously identified by McCabe et al. These deformation modes are implemented into a crystal plasticity finite element (CPFE) material model. A temperature dependent, dislocation density based law is implemented to describe the critical resolved shear stress on the different slip/twin systems. The strong anisotropic thermal expansion behaviour is taken into account to simulate the development of internal residual stresses following casting of the material. During cooling, the internal stresses in α-uranium are sufficient to induce plasticity. This effect is quantified using polycrystal simulations, in which first the temperature is decreased, then plastic relaxation takes place, followed by application of a mechanical load. The asymmetry between mechanical properties in tension and compression, due to the presence of twins, is investigated. The model is calibrated using stress strain curves and the lattice strain found from published neutron diffraction experiments carried out on textured samples at ISIS. The strength of the slip systems is found to be lower than in fine

grained material, while the strength of the twin system is similar to single crystals. The CPFE method allows the heterogeneity of the strain between neighbouring grains and its influence on the evolution of the internal stress state to be investigated.

1 Introduction

α-uranium is the stable phase of uranium up to 670°C and it is used for armour, projectiles and radiation shielding due to its high density (19.1 g/cm^3). The highly anisotropic crystal structure of α-uranium leads to anisotropic elastic coefficients [1] and thermal expansion coefficients [2]. Large thermal residual stresses develop during the casting process [3] that can facilitate fracture. The lattice of α-uranium is orthorhombic.

Dislocation glide and twinning create plastic deformation in α-uranium [4], depending on the temperature [5], loading conditions [6], grain shape [7] and size [6]. 8 active slip systems and 10 twin variants are present, which have very different critical resolved shear stresses (CRSS) [4, 8]. However, only the 2 variants of $\{130\}\langle 3\bar{1}0\rangle$ occupy a significant volume fraction of the crystal [9]. Fracture parallel to $\{172\}$ twin planes is observed [10], leading to the hypothesis that twin parting, similar to some minerals, is the main fracture initiation mechanism. However, cracks are also observed at the tip of twins and at the intersection between twins and grain boundaries [11]. To design and manufacture safe components, a quantitative model is necessary to predict the deformation and fracture behaviour of polycrystalline α-uranium.

Cast α-uranium has a mixed grain size, ranging from millimetres to hundreds of micrometres [12]. The grains are clustered into areas in which the misorientation is within 5°[13]. The recrystallization kinetics during heat treatment is affected by the texture [14] and rolling can transform the material into fine grained α-uranium [15], with grain sizes between 15 and 25 μm [15, 9]. Therefore, the effect of the grain size, spatial arrangement and texture needs to be quantified.

Previously, the elasto-plastic and visco-plastic self-consistent frameworks (EPSC and VPSC) have been used to model plastic deformation in α-uranium [16, 3]. These methods approximate a grain as a spherical inclusion inside a homogenised effective medium (HEM) [17]. In this paper, the crystal plasticity finite element (CPFE) method is used, which is able to model strain field inhomogeneities between neighbouring grains [18, 19]. The constitutive model is calibrated using stress strain curves and in-situ neutron diffraction experiments [13] carried out at the ENGIN-X beamline of the ISIS Neutron Source, Rutherford Appleton Laboratory, on coarse-grained α-uranium, with an average grain size of 200 μm.

A calibration of the values of the critical resolved shear stress (CRSS) for slip and twinning is carried out using polycrystal simulations. It shows that the CRSS for slip is lower than in fine grained specimens [16], while the CRSS for twinning is similar to single crystal specimens [5]. The Hall-Petch relationship turns out to be different for slip and twinning. Simulations of the quenching process are carried out to find the magnitude of the thermal residual stress for different textures. Finally, it is shown that grain clustering

leads to higher axial stresses.

2 Material Model

The finite strain crystal plasticity finite element framework is used [20], in which the deformation gradient is decomposed into elastic and plastic parts:

$$\boldsymbol{F} = \boldsymbol{F}_e \boldsymbol{F}_p \ . \tag{1}$$

The evolution of $\boldsymbol{F}_p$ takes into account the activity of the slip and twin systems [21]. The plastic velocity gradient is:

$$\boldsymbol{L}_p = \dot{\boldsymbol{F}}_p \boldsymbol{F}_p^{-1} = \left(1 - \sum_{\beta=1}^{N_{\text{twin}}} f_\beta\right) \sum_{\alpha=1}^{N_{\text{slip}}} \dot{\gamma}_\alpha \left(\boldsymbol{\sigma}\right) \boldsymbol{s}_\alpha \otimes \boldsymbol{n}_\alpha + \sum_{\beta=1}^{N_{\text{twin}}} \dot{f}_\beta \left(\boldsymbol{\sigma}\right) \gamma_\beta^{\text{twin}} \boldsymbol{s}_\beta \otimes \boldsymbol{n}_\beta \ , \tag{2}$$

where $\dot{\gamma}_\alpha$ is the shear rate on the slip system α, $\dot{f}_\beta$ is the rate of increase of the twin volume fraction on the twin system β and $\gamma_\beta^{\text{twin}}$ is the constant shear on the twin system β. Both $\dot{\gamma}_\alpha$ and $\dot{f}_\beta$ depend on the Cauchy stress $\boldsymbol{\sigma}$. $\dot{\gamma}_\alpha$ and $\dot{f}_\beta$ are described by a power law dependence on the resolved shear stress τ_α [16]. The twin volume fraction increases only if the resolved shear stress τ_β is positive. $\boldsymbol{s}_\alpha$ and $\boldsymbol{n}_\alpha$ are the slip direction and slip plane normal of the slip system α. $\boldsymbol{s}_\beta$ and $\boldsymbol{n}_\beta$ are the twin direction and twin plane normal of the twin system β. Table 1 contains the slip and twin systems used in the simulations and the lattice constants of α-uranium are reported in Table 3.

The Cauchy stress increment $\Delta\boldsymbol{\sigma}$ at every time step is proportional to the elastic strain increment [22]. The stiffness tensor of α-uranium at room temperature is [1]:

$$\mathbb{C} = \begin{bmatrix} 214.74 & 46.49 & 21.77 & 0 & 0 & 0 \\ 46.49 & 198.57 & 107.91 & 0 & 0 & 0 \\ 21.77 & 107.91 & 267.11 & 0 & 0 & 0 \\ 0 & 0 & 0 & 124.44 & 0 & 0 \\ 0 & 0 & 0 & 0 & 73.42 & 0 \\ 0 & 0 & 0 & 0 & 0 & 74.33 \end{bmatrix} \text{ GPa} \ , \tag{3}$$

and a linear decrease of the entries with temperature is imposed, as found in single crystals [5]. Thermal eigenstrains are considered using temperature dependent thermal expansion coefficients, as reported in [2]. The temperature dependent critical resolved shear stress $\tau_\alpha^c(T)$ of the slip systems is calculated using a dislocation density based model, developed by McCabe et al. [16]:

$$\tau_\alpha^c(T) = \left[\tau_\alpha^0 + 0.9 \ b_\alpha \mu_\alpha \sqrt{\rho_\alpha^{\text{for}}} - 0.086 \ b_\alpha \mu_\alpha \sqrt{\rho^{\text{sub}}} \log\left(b_\alpha \sqrt{\rho^{\text{sub}}}\right)\right] \exp\left(-\frac{(T - T_0)}{B_\alpha}\right) \ . \tag{4}$$

This represents the resolved shear stress at which the shear rate $\dot{\gamma}_\alpha$ has the same magnitude as the externally applied deformation shear rate. ρ_α^{for} is the forest dislocation density on the slip system α and ρ^{sub} the dislocation density in the substructures [23]. The critical

Slip system	$\boldsymbol{s}_\alpha^0$	$\boldsymbol{n}_\alpha^0$	b_α (nm)	μ_α (GPa)
$\alpha = 1$ (wall)	$[100]$	(010)	0.285	74.330
$\alpha = 2$ (floor)	$[100]$	(001)	0.285	73.420
$\alpha = 3$ (chimney)	$[1\bar{1}0]$	(110)	0.651	92.255
$\alpha = 4$ (chimney)	$[110]$	$(1\bar{1}0)$	0.651	92.255
$\alpha = 5$ (roof)	$[1\bar{1}2]$	(021)	1.185	115.67
$\alpha = 6$ (roof)	$[\bar{1}\bar{1}2]$	(021)	1.185	115.67
$\alpha = 7$ (roof)	$[112]$	$(0\bar{2}1)$	1.185	115.67
$\alpha = 8$ (roof)	$[1\bar{1}\bar{2}]$	$(0\bar{2}1)$	1.185	115.67

Twin system	$\boldsymbol{s}_\beta^0$	$\boldsymbol{n}_\beta^0$
$\beta = 1$	$[3\bar{1}0]$	(130)
$\beta = 2$	$[\bar{3}\bar{1}0]$	$(\bar{1}30)$

Table 1: Miller indices of the slip and twin systems used in the model [16]. Burgers vectors and projected shear moduli [1, 16].

resolved shear stress, τ_β, of the twin systems is assumed to be constant. The time evolution of the dislocation densities is based on a multiplication-annihilation formalism, as reported in [16], and is calibrated to reproduce the hardening rate [16]. b_α is the Burgers vector and μ_α the projected shear modulus of the slip system α [23, 16]. The values are in Table 1.

Three different sets of parameters for the constant friction stresses τ_α^0 and τ_β, for plastic slip and twinning, are compared in the present study. They are reported in Table 2. The fine grained parameters correspond to 12.5 μm grain size [16], while the single crystal parameters have been obtained using specimens of length 2.5-3 mm [5]. The present material has an average grain size of 200 μm [13] and the parameters in the present study have been calibrated using stress-strain curves and neutron diffraction experiments. The

τ_α^0 (MPa)	Wall	Floor	Chimney	Roof	{130} Twin
Fine grained (McCabe et al. [16])	60	270	295	270	300
Single crystal (Daniel et al. [5])	4	80	168	N/A	25
Coarse grained (present study)	7	10	35	235	25

Table 2: Constant friction stress for the different models.

CRSS for dislocation slip decreases exponentially with temperature, as in equation (4). B_α is a thermal activation parameter [24] and $T_0 = 293$ K is the reference temperature. Model parameters are reported in Table 3.

Polycrystal simulations are carried out by assigning a different rotation matrix $\boldsymbol{R}$ to every grain, which is used to rotate the directions and normals of the slip and twin systems in Table 1.

The model is implemented as a UMAT (user material subroutine) for Abaqus [18], which solves the stress equilibrium equation. The variables ρ_α^{for}, ρ^{sub} and f_β are updated at every time increment. A Newton-Raphson algorithm is used to find the plastic velocity gradient $\boldsymbol{L}_p$ that is compatible with the stress increment and with the elasto-plastic decomposition in equation (1). At every time step the crystal rotation matrix $\boldsymbol{R}$ is updated

Lattice constant (a) [26]	0.2852 nm
Lattice constant (b) [26]	0.5865 nm
Lattice constant (c) [26]	0.4945 nm
Magnitude of shear due to twinning ($\gamma_\beta^{\text{twin}}$) [4]	0.299
Thermal activation parameter for slip (B_α) [24]	140 K

Table 3: Model parameters.

using the continuum elastic spin matrix [25].

3 Polycrystal simulations and elastic lattice strain

To introduce thermal residual stresses, simulations are divided into three phases: first a polycrystal with 8000 ($20 \times 20 \times 20$) cubic grains is cooled down from 400°C to room temperature in 10 s [27], as shown in Figure 1 (a); then, 7000 external grains are removed and the system relaxes for 100 s; finally, deformation is applied along the x axis on the 1000 ($10 \times 10 \times 10$) grains that are in the centre of the original geometry, as shown in Figure 1 (b). The original size of the cubic representative volume is 6000 μm.

The boundary conditions during the three phases are the following. Given the origin O in Figure 1 (a), the surfaces $x = 0$, $y = 0$ and $z = 0$ have zero perpendicular displacement during quenching. During the relaxation phase, given the origin O in Figure 1 (b), the newly created free surfaces $x = 0$, $y = 0$ and $z = 0$ have zero velocity along x, y and z respectively. Finally, pure axial tension or compression along the x axis is applied, up to 1% strain, as shown in Figure 1 (b). The initial value of the dislocation densities ρ_α^{for} and ρ^{sub} is 10^{10} m^{-2} and no twins are present at the beginning of the simulations.

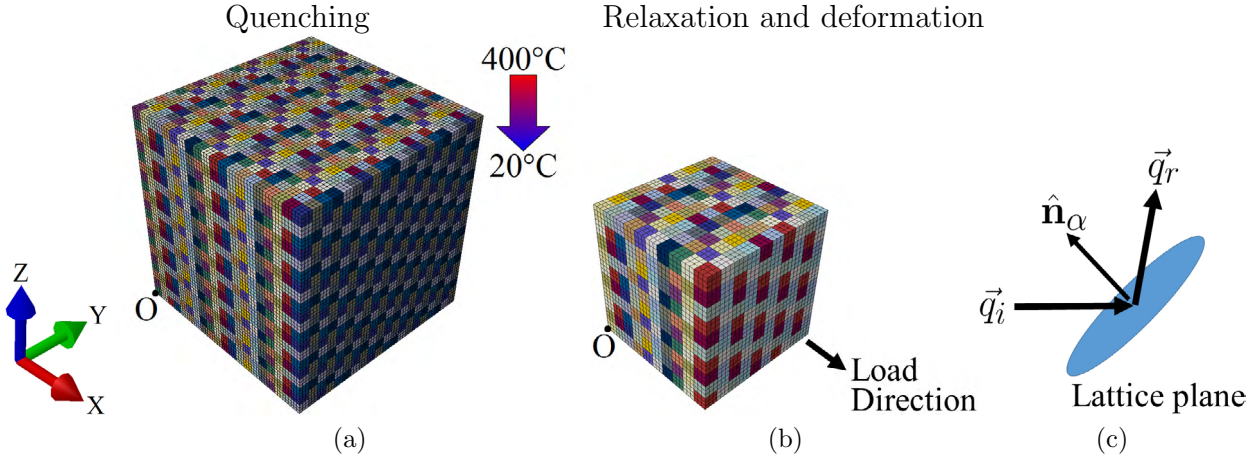

Figure 1: (a) 8000 grains representative volume and mesh during quenching. (b) 1000 grains in the inner part of the representative volume during deformation and load direction. (c) Directions $\vec{\boldsymbol{q}}_i$ and $\vec{\boldsymbol{q}}_r$ of the incident and diffracted neutron beam.

The Green-Lagrange elastic strain tensor is calculated in the crystal lattice coordinate system and its diagonal components are compared with the neutron diffraction experi-

ments. These components will be called (100), (010) and (001) lattice strain in this paper. A grain selection algorithm is developed that selects the grains in which a specific family of lattice planes reflects the neutron beam towards the detector area. The incident neutron beam has direction $\vec{\boldsymbol{q}}_i = \left[1/\sqrt{2}; 1/\sqrt{2}; 0\right]$ and it is reflected by a lattice plane towards the direction $\vec{\boldsymbol{q}}_r$, as shown in Figure 1 (c). The direction $\vec{\boldsymbol{q}}_d = \left[-1/\sqrt{2}; 1/\sqrt{2}; 0\right]$, which is perpendicular to the incident beam, points towards the centre of the detector. Thus, only neutrons diffracted by lattice planes with normals approximately parallel to the load axis are detected. The horizontal detector coverage in the x-y plane is $\pm 14°$, while the vertical coverage, out of the x-y plane, is $\pm 21°$. The simulated Green-Lagrange elastic strain tensor is averaged over the selected grains. For instance, the (100) elastic lattice strain is averaged over grains in which the (100) lattice planes reflect the neutron beam towards the detector.

In the present study, two specimens with different textures C1 and T1 are analysed, as shown in Figure 2 (a) and (b). From these textures, a distribution for the orientations of the 1000 grains in the central part of the representative volume can be obtained, as depicted in Figure 2 (c) for the T1 texture. Each point represents the orientation of the load direction (x axis in the sample coordinate system) in the crystal lattice coordinate system. The outer 7000 grains have a random texture. Two types of spatial arrangement of the 1000 central grains are investigated to understand the effect of grain clustering observed experimentally [13]: the first one has a spatially random grain distribution (RGD); in the second one (GC), the orientations belonging to the two peaks of the probability distribution functions in Figures 2 (a)-(b) ({350} and {190} for the C1 texture, {115} and {312} for the T1 texture) are assigned to grains with low and high z coordinates in Figure 1 (b) respectively. In this second case, the representative volume is similar to a bicrystal with two grains arranged parallel to the load direction.

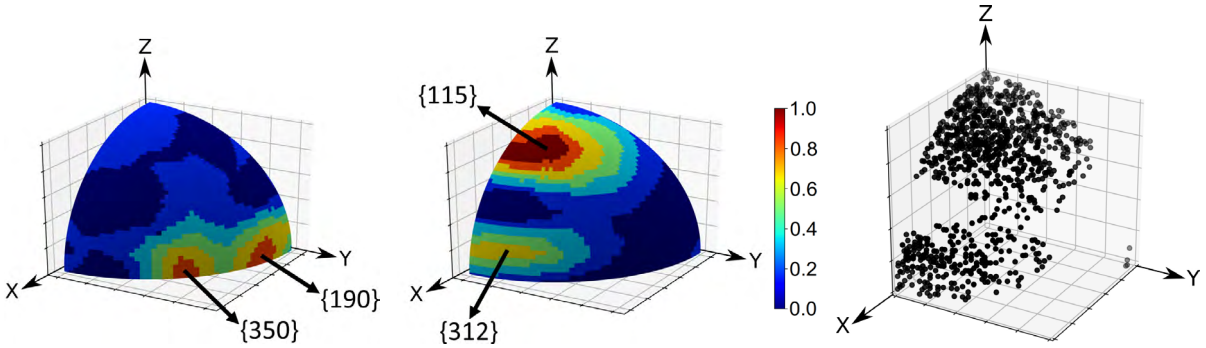

(a) (b) (c)

Figure 2: (a) Texture of the sample C1, deformed in compression. (b) Texture of the sample T1, deformed in tension. (c) Random distribution of grain orientations, generated with the probability distribution function in (b).

4 Results

4.1 Stress-strain curves

The simulated axial stress on the load surface in Figure 1 (b) is shown in Figure 3 using different material parameters. The parameters for the present study on coarse grained α-uranium in Table 2 are calibrated to fit both the tension and compression experiments. The fine grained parameters lead to the highest stress and also using single crystal parameters the stress is overestimated. If the grain clustering is considered, a higher stress is obtained for the T1 texture.

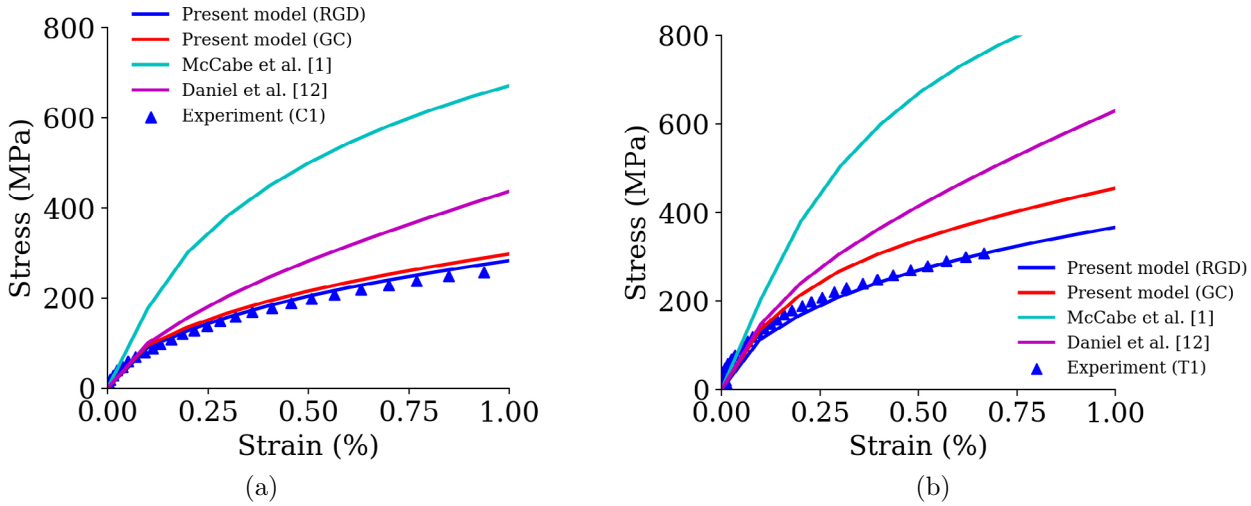

Figure 3: Simulated and experimental stress-strain curves (a) for compression (C1 texture) and (b) for tension (T1 texture).

The T1 texture shows higher stress because of the presence of the {115} grains, which have less active slip and twin modes. The {130} twin system is active in tension for (100)-oriented grains, prevalent in the T1 texture, and in compression for (010)-oriented grains, prevalent in the C1 texture. In the present model, the twin system gives the highest contribution to plastic deformation, followed by wall and floor slip.

The simulated twin volume fraction after quenching, between 5% and 6%, is comparable to that observed by EBSD measurements on the same sample [13]. This provides another validation for the model parameters for coarse grained α-uranium in Table 2.

4.2 Elastic lattice strain

The simulated (100) and (010) elastic lattice strain as a function of the axial stress is shown in Figures 4 and 5. The elastic lattice strain is a measure of the microscopic stress in a grain family; therefore, saturation of the elastic lattice strain indicates that plastic deformation has started only in that grain family.

The present model, without the grain clustering, is the one that best fits the (100)

elastic lattice strain data. The saturation behaviour in the T1 sample is explained with the activation of the {130} twin system, which is not active in compression (sample C1). No saturation of the elastic lattice strain is present if the fine grained material parameters (McCabe et al. [16]) are used because the CRSS for twinning is higher than for slip.

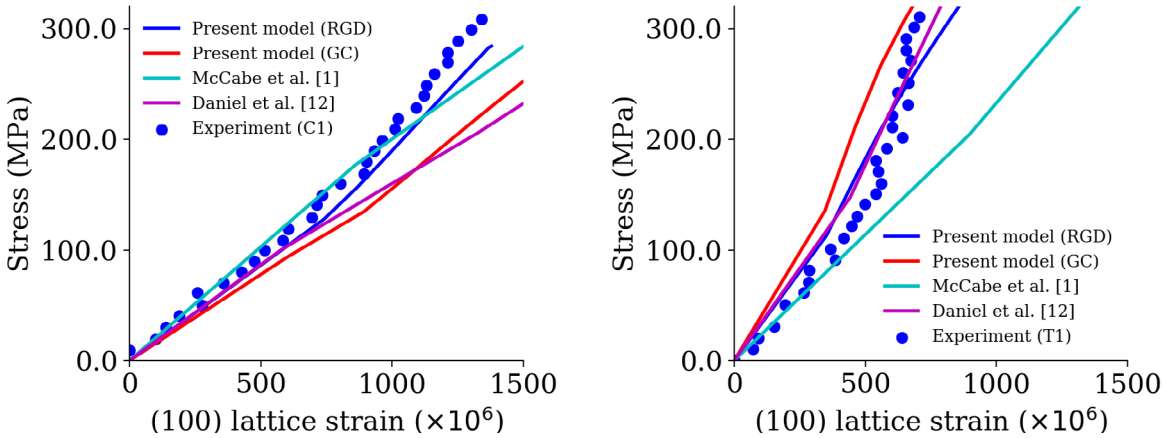

Figure 4: Simulated and measured (100) elastic lattice strain for (a) C1 sample (compression) and (b) T1 sample (tension).

The present model with the grain clustering is the one that best fits the (010) elastic lattice strain of the T1 sample, as shown in Figure 5 (b); however, the saturation behaviour of the C1 sample is not well captured. Twinning is expected in (010)-oriented grains in compression; however, the simulations indicate that both grain families {350} and {190} in Figure 2 (a) have similar plastic deformation due to twinning. Therefore, the simulated mechanical behaviour of the C1 texture is more similar to a single crystal and the microscopic elastic lattice strain is always proportional to the macroscopic stress.

4.3 Thermal residual stress

The calibrated model is used to study the thermal residual stress development during quenching. The Von Mises stress averaged over the 1000 grains in the central part of the representative volume is shown in figure 6 as a function of temperature. The stress reached after cooling is enough to activate the easiest slip modes as well as twinning. It is negligibly higher for the C1 texture and does not depend strongly on the spatial arrangement of the grains.

5 Discussion and conclusions

The agreement between the present model and the experimental results for coarse grained α-uranium shows that the CRSS for slip is smaller than for fine grained α-uranium

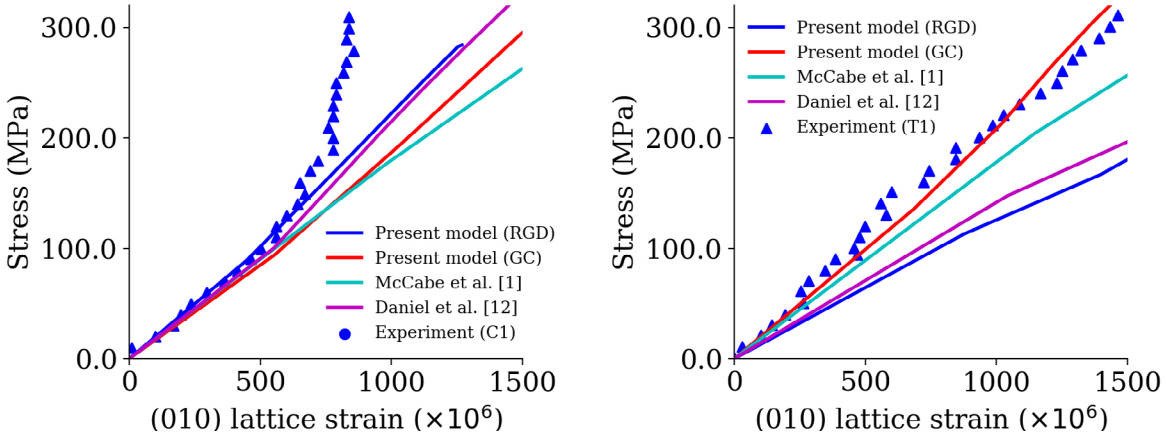

(a) (b)

Figure 5: Simulated and measured (010) elastic lattice strain for (a) C1 sample (compression) and (b) T1 sample (tension).

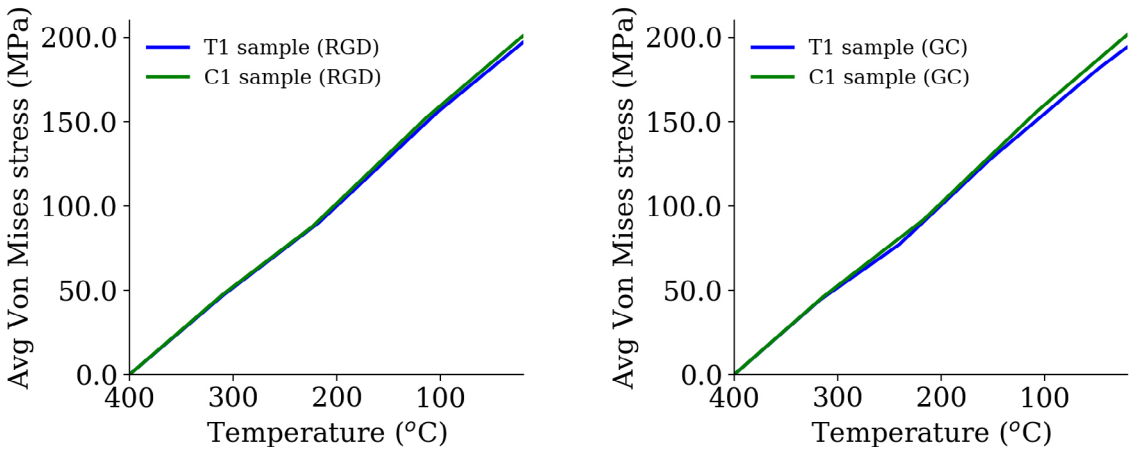

(a) (b)

Figure 6: Simulated average Von Mises stress during quenching in case of (a) spatially random grain distribution (RGD) and (b) grain clustering (GC) for the C1 and T1 textures.

[16]. As shown in Section 4.2, the activation of the {130} twin system leads to the tension-compression asymmetry in the (100) elastic lattice strain. This asymmetry is reproduced by the simulations only if the CRSS for twinning is smaller than for chimney and roof slip. The calibrated value of the twinning CRSS (25 MPa) is the same as the value found in single crystals [5] and leads to a twin volume fraction after quenching comparable to the value measured with EBSD [13]. The saturation of the (100) elastic lattice strain in tension

takes place at a macroscopic stress close to 115 MPa, corresponding to a resolved shear stress on the twin system of approximately 54 MPa. This stress is higher than the CRSS (25 MPa) for twinning and shows CPFE simulations are needed to avoid overestimation of the CRSS when analysing neutron diffraction data.

The present simulations suggest that the Hall-Petch dependence [28, 6] is strong for the slip and twin systems of α-uranium for grain size between 12.5 μm and 200 μm. However, there is little grain size dependence of the CRSS for twin formation from 200 μm to millimetre sized single crystals [5].

The formation of grain clusters can significantly change the mechanical properties, as shown by the simulated stress-strain curves in Figure 3 and by the elastic lattice strain in figure 5. The saturation behaviour of the (010) elastic lattice strain in compression, which is not captured by the simulations, may be due to the presence of harder grains, bearing part of the macroscopic stress but placed outside of the neutron beam cross section. The simulations show that the C1 texture, with two grain families at {350} and {190}, has a behaviour similar to a single crystal and the plastic deformation distribution is almost uniform in the two grain families.

In conclusion, a crystal plasticity model is outlined to describe slip and twinning in coarse grained α-uranium. The model predicts not only the stress-strain curves, but also the elastic lattice strain in textured samples, as measured by neutron diffraction experiments. The constitutive model can be applied to find the thermal residual stress after quenching and represents a first step towards understanding the interplay between plasticity and fracture in α-uranium.

Acknowledgements

The authors acknowledge financial support of AWE plc for this research, program manager: Dr John Askew. The authors would like to thank Philip Earp and Prof James Marrow for discussion about their experimental techniques and results. ET acknowledges support from the Engineering and Physical Sciences Research Council under Fellowship grant EP/N007239/1.

REFERENCES

[1] E. S. Fisher and H. J. McSkimin. Adiabatic elastic moduli of single crystal alpha uranium. *Journal of Applied Physics*, 29(10):1473–1484, 1958.

[2] Lowell T. Lloyd and C.S. Barrett. Thermal expansion of alpha uranium. *Journal of Nuclear Materials*, 18(1):55 – 59, 1966.

[3] C.A. Calhoun, J.A. Wollmershauser, D.W. Brown, R.P. Mulay, E. Garlea, and S.R. Agnew. Thermal residual strains in depleted α-U. *Scripta Materialia*, 69(8):566 – 569, 2013.

[4] R.W Cahn. Plastic deformation of alpha-uranium; twinning and slip. *Acta Metallurgica*, 1(1):49 – 70, 1953.

[5] J.S Daniel, B Lesage, and P Lacombe. The influence of temperature on slip and twinning in uranium. *Acta Metallurgica*, 19(2):163 – 173, 1971.

[6] H. Inouye and S.C. Schaffhauser. Low-temperature ductility and hydrogen embrittlement of uranium - a literature review. *ORNL-TM-2563*, 1969.

[7] D.M.R. Taplin and J.W. Martin. The effect of grain shape on the tensile properties of α uranium. *Journal of Nuclear Materials*, 10(2):134 – 139, 1963.

[8] C.A. Calhoun, E. Garlea, T.A. Sisneros, and S.R. Agnew. In-situ neutron diffraction characterization of temperature dependence deformation in -uranium. *Journal of Nuclear Materials*, 502:60 – 67, 2018.

[9] D.W. Brown, M.A.M. Bourke, B. Clausen, D.R. Korzekwa, R.C. Korzekwa, R.J. McCabe, T.A. Sisneros, and D.F. Teter. Temperature and direction dependence of internal strain and texture evolution during deformation of uranium. *Materials Science and Engineering: A*, 512(1):67 – 75, 2009.

[10] R.D. Field, R.J. McCabe, D.J. Alexander, and D.F. Teter. Deformation twinning and twinning related fracture in coarse-grained -uranium. *Journal of Nuclear Materials*, 392(1):105 – 113, 2009.

[11] D.M.R. Taplin. *J. Aust. Inst. Met.*, 12:32, 1967.

[12] E. Garlea, R.L. Bridges, V.O. Garlea, D.A. Carpenter, M.A. Hemphill, and J.S. Morrell. Characterization of a grain size refinement process in cast uranium. *Materials Science and Engineering: A*, 559:210 – 216, 2013.

[13] P Earp, S Kabra, J Askew, and T J Marrow. Lattice strain and texture development in coarse-grained uranium a neutron diffraction study. *Journal of Physics: Conference Series*, 1106(1):012012, 2018.

[14] R.J. McCabe, A.W. Richards, D.R. Coughlin, K.D. Clarke, I.J. Beyerlein, and M. Knezevic. Microstructure effects on the recrystallization of low symmetry alpha-uranium. *Journal of Nuclear Materials*, 465:189 – 195, 2015.

[15] Miroslav Zecevic, Marko Knezevic, Irene J. Beyerlein, and Rodney J. McCabe. Origin of texture development in orthorhombic uranium. *Materials Science and Engineering: A*, 665:108 – 124, 2016.

[16] R.J. McCabe, L. Capolungo, P.E. Marshall, C.M. Cady, and C.N. Tom. Deformation of wrought uranium: Experiments and modeling. *Acta Materialia*, 58(16):5447 – 5459, 2010.

[17] J. W. Hutchinson and Robert Hill. Elastic-plastic behaviour of polycrystalline metals and composites. *Proceedings of the Royal Society of London. A. Mathematical and Physical Sciences*, 319(1537):247–272, 1970.

[18] T.O. Erinosho, A.C.F. Cocks, and F.P.E. Dunne. Texture, hardening and non-proportionality of strain in bcc polycrystal deformation. *International Journal of Plasticity*, 50:170 – 192, 2013.

[19] F. Roters, M. Diehl, P. Shanthraj, P. Eisenlohr, C. Reuber, S.L. Wong, T. Maiti, A. Ebrahimi, T. Hochrainer, H.-O. Fabritius, S. Nikolov, M. Frik, N. Fujita, N. Grilli, K.G.F. Janssens, N. Jia, P.J.J. Kok, D. Ma, F. Meier, E. Werner, M. Stricker, D. Weygand, and D. Raabe. DAMASK the Düsseldorf advanced material simulation kit for modeling multi-physics crystal plasticity, thermal, and damage phenomena from the single crystal up to the component scale. *Computational Materials Science*, 2018.

[20] Suchandrima Das, Felix Hofmann, and Edmund Tarleton. Consistent determination of geometrically necessary dislocation density from simulations and experiments. *International Journal of Plasticity*, 109:18 – 42, 2018.

[21] Surya R. Kalidindi. Incorporation of deformation twinning in crystal plasticity models. *Journal of the Mechanics and Physics of Solids*, 46(2):267 – 290, 1998.

[22] F.P.E. Dunne, D. Rugg, and A. Walker. Lengthscale-dependent, elastically anisotropic, physically-based hcp crystal plasticity: Application to cold-dwell fatigue in ti alloys. *International Journal of Plasticity*, 23(6):1061 – 1083, 2007.

[23] L. Capolungo, I.J. Beyerlein, G.C. Kaschner, and C.N. Tom. On the interaction between slip dislocations and twins in hcp zr. *Materials Science and Engineering: A*, 513-514:42 – 51, 2009.

[24] Miroslav Zecevic, Marko Knezevic, Irene J. Beyerlein, and Rodney J. McCabe. Texture formation in orthorhombic alpha-uranium under simple compression and rolling to high strains. *Journal of Nuclear Materials*, 473:143 – 156, 2016.

[25] Fionn Dunne and Nik Petrinic. *Introduction to computational plasticity*. Oxford university press, 2006.

[26] C. W. Tucker. The crystal structure of the β phase of uranium. *Acta Crystallographica*, 4(5):425–431, Sep 1951.

[27] Marko Knezevic, Laurent Capolungo, Carlos N. Tom, Ricardo A. Lebensohn, David J. Alexander, Bogdan Mihaila, and Rodney J. McCabe. Anisotropic stress strain response and microstructure evolution of textured α-uranium. *Acta Materialia*, 60(2):702 – 715, 2012.

[28] E O Hall. The deformation and ageing of mild steel: III discussion of results. *Proceedings of the Physical Society. Section B*, 64(9):747–753, sep 1951.